Quantitative estimation of nonmonotonic residual stress depth-profiles using an extended Kypris-Jiles model of the magnetic Barkhausen noise spectrum

Aitor Lasaosa, Kizkitza Gurruchaga, Fernando Arizti, and Ane Martínez-de-Guerenu

Citation: Journal of Applied Physics **123**, 033904 (2018);
View online: https://doi.org/10.1063/1.5002074
View Table of Contents: http://aip.scitation.org/toc/jap/123/3
Published by the American Institute of Physics

Quantitative estimation of nonmonotonic residual stress depth-profiles using an extended Kypris-Jiles model of the magnetic Barkhausen noise spectrum

Aitor Lasaosa,[1,2,a)] Kizkitza Gurruchaga,[1,2,b)] Fernando Arizti,[1,2,c)] and Ane Martínez-de-Guerenu[1,2,d)]
[1]*Ceit, Manuel Lardizabal 15, 20018 Donostia/San Sebastián, Spain*
[2]*Universidad de Navarra, Tecnun, Manuel Lardizabal 13, 20018 Donostia/San Sebastián, Spain*

(Received 29 August 2017; accepted 26 December 2017; published online 17 January 2018)

Using nondestructive techniques to quantitatively estimate residual stresses along the depth is necessary to improve the ability to predict the real fatigue life of pieces for many applications. Magnetic Barkhausen noise has been proven to successfully estimate the residual stress at the surface produced by machining, plastic deformation, phase transformation or surface treatments such as shot peening, also allowing one to obtain information of the residual stress depth-profile in shot peened pieces which presented similar depth-profile shapes. However, residual stress depth-profiles with nonmonotonic or different shapes have not been successfully estimated. In the present study, an extended approach is developed in order to estimate these stresses independent of the shape of the residual stress depth-profile. The approach proposed here improves an existing model of the Barkhausen noise spectrum (Kypris-Jiles model) by adding the effect of the attenuation of the applied magnetic field on the Barkhausen noise. This extended approach is used to estimate the residual stress depth-profiles of samples with different depth-profiles using a calibration process. The approach is validated by estimating the residual stress depth-profiles, with errors smaller than 70 MPa in a depth of 130 μm, in all the samples studied. *Published by AIP Publishing.*
https://doi.org/10.1063/1.5002074

I. INTRODUCTION

Estimating fatigue life is important in many fields of engineering in order to carry out an optimum maintenance and inspection plan for parts in diverse industrial sectors. Residual stresses are one of the critical features that need to be known in order to estimate the fatigue life cycle properly.[1] The so called residual stresses are stresses present in the parts once the source of load is removed and they could also be produced throughout the manufacturing process. In many applications, the parts are shot peened to obtain compressive residual stresses and thus increase the parts' life cycle. However, the presence of compressive residual stresses at the beginning of the life cycle does not assure that the residual stresses will remain constant over time. In fact, it has been observed that a relaxation of the residual stresses occurs over time and also that external factors could introduce new residual stresses that would change the fatigue life of the part.[1,2] Therefore, in order to improve the life cycle prediction, it is important to estimate the residual stress depth-profile at the beginning of the life cycle, but it is also important to monitor the changes in the residual stress depth-profile during service by nondestructive techniques.

In the present work, the magnetic Barkhausen noise (MBN) technique is used to estimate the residual stress depth-profiles due to its well-known sensitivity to stresses,[3–16] a capability that has been shown so far to attain information from different depths.[3,4,6,9–12,14,17,18] Another point in its favor is the portability of MBN measurement systems relative to conventional nondestructive residual stress depth-profile measurement systems, such as neutron diffraction or synchrotron X-ray diffraction (XRD). The MBN technique measures the signal produced by the movement of magnetic domain walls inside ferromagnetic materials when a time-varying magnetic field is applied. In general terms, for steels with positive magnetostriction, it has been observed that the MBN signal amplitude increases when the stress is tensile and decreases when the stress is compressive.[3–16] Moreover, the MBN signal emitted inside the material is attenuated by eddy current damping, as it has to travel through the material to reach a MBN sensor located at the surface of the material.

By studying the MBN at different frequency bands, information from different depths can be obtained,[3,6,9–12,14,18] and by combining this with the relation between the stress and the MBN amplitude, it is possible to obtain an estimation of residual stresses present at different depths of the material.[3,6,9–12,14] However, the approaches used so far to obtain these approximations present drawbacks: some cannot estimate nonmonotonic residual stress depth-profiles with different shapes,[3,6,9,11,14] and others, even though their theoretical frameworks are promising, have not yet been proven to successfully estimate nonmonotonic residual stress depth-profiles in real samples.[10,12]

In the present work, the objective is to develop an approach that is able to estimate nonmonotonic residual stress depth-profiles independent of their shapes (e.g., monotonic, nonmonotonic or different) by taking MBN measurements at

[a)]E-mail: alasaosa@ceit.es
[b)]E-mail: kgurruchaga@ceit.es
[c)]E-mail: fernando@ceit.es
[d)]E-mail: amartinez@ceit.es

the surface of the part. For this purpose, the approach and model proposed by Kypris *et al.*[10] (hereafter referred to as the "Kypris-Jiles model") are taken as the starting point, as they present a theoretical framework for estimating the residual stress depth-profile independent of the shape of the depth-profile. As this model had not been used before for estimation of nonmonotonic residual stress depth-profiles, in the present work, it was applied to check its applicability.

Additionally, an extended approach that modifies the Kypris-Jiles MBN magnitude spectrum model is proposed here. The extended model includes an additional effect on MBN attenuation with reference to the attenuation of the applied magnetic field.[19–21] Furthermore, the discretization in the depth direction of the sample made to fit the model to the MBN measurements is modified to take into account the large variation produced by residual stresses on the MBN amplitude. Lastly, the extended theoretical approach is validated using samples with different residual stress depth-profiles. Using this extended approach and the spectrum of the MBN acquired at the surface of each sample, a qualitative estimation of their residual stress depth-profiles is obtained. Moreover, after a calibration process involving the qualitative values obtained with the extended approach and the residual stress depth-profiles obtained by destructive means on some reference samples, a quantitative estimation of the nonmonotonic residual stress depth-profile in other samples is achieved.

II. THEORY

A. Barkhausen noise magnitude spectrum model

The Kypris-Jiles model of the Barkhausen noise magnitude spectrum[10] is based on the attenuation suffered by the MBN signal as it travels from the emission point inside the material to the surface due to eddy current damping, which is described by the following equation:[3,6,9–12,18]

$$V(x,\omega) = V_{orig}(\omega) * \exp\left(\frac{-x}{\delta}\right), \tag{1}$$

where V_{orig} is the MBN emitted at a depth x from the surface, ω is the angular frequency of the emitted signal, and δ, also known as skin depth, is the distance at which the signal is attenuated by a factor of e^{-1} and is given by the following equation:

$$\delta = \sqrt{\frac{2\rho}{\omega\mu}}, \tag{2}$$

where ρ and μ are the electrical resistivity and magnetic permeability of the material, respectively, and ω is the angular frequency of the emitted signal.

The $V_{orig}\ (\omega)$ is considered as white noise in Ref. 10 because the parameter associated with the magnetizing rate ($c = \sqrt{\mu\omega/2\pi^2\rho} * 0.1356w$, where w is the width of the section) is greater than 0, ($c = 0.14$), so the V_{orig} on each ω has the same value. Furthermore, in Ref. 10, it is believed that the V_{orig} is the only function of the residual stress (σ) present at the depth where this V_{orig} is emitted ($V_{orig}\ (\sigma)$) and the μ depends on the average residual stress ($\overline{\sigma}$) from the depth from which this V_{orig} is emitted to the surface where the sensor is located (which is called effective magnetic permeability ($\mu_{eff}(\overline{\sigma})$ from this point on). This is so, taking into consideration that other material properties such as microstructure are nearly constant along the depth and that their impact on the V_{orig} value and μ_{eff} value are negligible. Therefore, Eq. (1) can be represented as follows:

$$V(x,\omega,\sigma) = V_{orig}(\sigma) * \exp\left(-\zeta(\overline{\sigma})\, x \sqrt{\omega}\right), \tag{3}$$

$$= V_{orig}(\sigma) * \mathrm{f}_1\left(x,\omega,\zeta(\overline{\sigma})\right), \tag{4}$$

where $\zeta(\overline{\sigma}) = \sqrt{\mu_{eff}(\overline{\sigma})/2\rho)}$ is introduced for mathematical tractability and is responsible for the rate of attenuation due to eddy current damping.

The Kypris-Jiles model represents the measured MBN magnitude spectrum at each frequency ($V_{sensor,\omega}$) with the following equation, considering the samples to be formed by discrete layers of Δx width in the depth direction, where each of these layers is considered to be homogeneous:

$$\begin{aligned} V_{Sensor,\omega} = {} & \left[V_{\mathrm{orig}\,0}(\sigma_0) * \mathrm{f}_1(x_0,\omega,\zeta_0(\overline{\sigma}_0))\right. \\ & + V_{\mathrm{orig}\,1}(\sigma_1) * \mathrm{f}_1(x_1,\omega,\zeta_1(\overline{\sigma}_1)) + \cdots \\ & + V_{\mathrm{orig,n-1}}(\sigma_{n-1}) * \mathrm{f}_1 \\ & \left.(x_{n-1},\omega,\zeta_{n-1}(\overline{\sigma}_{n-1}))\right] * \omega^{-0.2}, \end{aligned} \tag{5}$$

where $V_{orig,0}$, $V_{orig,1}$,..., and $V_{orig,n-1}$ are the MBN values at the origin emitted at the layers located at distances x_0, x_1,... and x_{n-1} (where x_{n-1} is the maximum depth analyzed) from the surface as a function of the residual stress (σ) present in each layer. ζ_0, ζ_1,..., and ζ_{n-1} are responsible for the rate of attenuation from each layer and $\omega^{-0.2}$ is a heuristic term added in Ref. 10 for a better match with the magnitude spectrum.

In the extended model introduced here, the assumptions made in Ref. 10 to obtain Eq. (5) are also considered: white noise for V_{orig} is assumed since the parameter associated with the magnetizing rate is very similar to the value in Ref. 10 {$c = 0.12$, considering ρ and μ to be similar to the properties of iron [$\rho = 0.3175\ \mu\Omega$ m, $\mu = 500{*}\mu_0$ (Refs. 22 and 23)], and $w = 0.025$ m}; the parameters V_{orig} and ζ are only considered to be functions of σ and $\overline{\sigma}$, respectively, considering as a starting point other material properties such as microstructure to be constant. In case the microstructure of the samples changed and its influence was significant, the relation between the V_{orig} and the residual stresses would become worse, becoming inexistent in case the influence of the stresses on the V_{orig} were negligible comparing to the influence of the microstructural change.

In order to take into account the effect that the attenuation of the applied magnetic field has on the V_{orig} term as this field penetrates the material, an additional term is added to Eq. (5). This attenuation is a well-known effect that reduces the applied magnetic field signal as it travels through the material in a way that is similar to the attenuation of the MBN signal, but not only is the eddy current damping involved, but so are hysteresis losses, magnetic viscosity,

demagnetizing factor, etc.[19–21] The consequence of this attenuation is that the MBN signals emitted further from the surface present lower amplitudes than the MBN signals emitted nearer the surface. This happens because the MBN amplitude is a function of the time derivative of the applied magnetic field[24,25] and this time derivative decreases as the applied magnetic field decreases.

In order to add this effect to the model, as an approximation, it is considered that the applied magnetic field is attenuated exponentially due to the eddy current damping and other factors are ignored. Then, the relationship between the exponential attenuation of the applied field and the MBN amplitude are considered to be linear, yielding the following equation:

$$\begin{aligned} &\textit{Magnetic field attenuation factor} \\ &= k*\exp\left(-\zeta_n(\overline{\sigma}_n)x_n\sqrt{\omega_{exc}}\right), \quad (6) \\ &= k*f_2(x_n, \omega_{exc}, \zeta_n(\overline{\sigma}_n)), \quad (7) \end{aligned}$$

where k is an unknown constant for all layers representing the effect of the derivative of the magnetic field in the MBN amplitude, x_n is the distance from the surface to each layer, ζ_n is responsible for the rate of attenuation from each layer located at x distance from the surface, and ω_{exc} is the angular excitation frequency. This factor multiplies each $V_{orig,n}$ and modifies Eq. (5) without the heuristic term $\omega^{-0.2}$ as follows:

$$\begin{aligned} V_{Sensor,\omega} = &\left[V_{\mathrm{orig},0}(\sigma_0)*\mathrm{f}_1(x_0, \omega, \zeta_0(\overline{\sigma}_0))*\mathrm{f}_2(x_0, \omega_{exc}, \zeta_0(\overline{\sigma}_0))\right. \\ &+V_{\mathrm{orig},1}(\sigma_1)*\mathrm{f}_1(x_1, \omega, \zeta_1(\overline{\sigma}_1))*\mathrm{f}_2(x_1, \omega_{exc}, \zeta_1(\overline{\sigma}_1)) \\ &+\cdots+V_{\mathrm{orig},n-1}(\sigma_{n-1})*\mathrm{f}_1(x_{n-1}, \omega, \zeta_{n-1}(\overline{\sigma}_{n-1})) \\ &\left.*\,\mathrm{f}_2(x_{n-1}, \omega_{exc}, \zeta_{n-1}(\overline{\sigma}_{n-1}))\right]*k. \quad (8) \end{aligned}$$

B. Residual stress estimation approach

The extended approach for estimating residual stress depth-profiles proposed in the present study consists of 3 stages that have been applied with the extended and the bare Kypris-Jiles models of the measured MBN magnitude spectrum:

(a) *Fitting the model to the measured MBN magnitude spectrum*: in order to perform the fitting, some considerations should be taken. First of all, a number of parameters should be taken as the ones varying to perform the fitting. In this case, the V_{orig}, the ζ, and the k (only for the extended Kypris-Jiles model) parameters are used. Second, the $x_{n\text{-}1}$ depth should be set. For the bare Kypris-Jiles model, this is done using Eq. (2), as proposed in Ref. 10. However, when there is a gradient in the material properties along the depth that could change the amplitude of the MBN greatly, this depth could be slightly different.[25,26] In this case, as the residual stresses could vary in high extent, the $x_{n\text{-}1}$ of the extended model is not calculated as the depth coming from Eq. (2), but as a depth 1.8 times greater, in order to consider that it is possible to have an amplitude difference at the MBN signal of six fold greater along the depth, due to change of residual stresses.[27] Finally, the Eqs. (5) and (8) are fitted using a nonlinear least squares algorithm for the bare and extended models, respectively.

(b) *Linear calibration of V_{orig} parameters with X-ray measurements of residual stresses*: in this step, calibration functions are obtained for each depth. These functions are calculated using samples with known and different residual stress depth-profiles. A linear regression function for each depth ($\sigma_n = a_n*V_{orig\,n} + b_n$, where a_n and b_n are constant for each depth) is calculated using the V_{orig} and residual stress values of the samples at those depths. V_{orig} is used because it is the only parameter related with the residual stress value at each depth, since the ζ is related with the average value of the residual stress from the surface to each depth.

(c) *Validation of the calibration functions*: here, V_{orig} and residual stress values of known sample or samples not used at the calibration step are used in order to validate the functions for each depth. The V_{orig} value and the calibration function from each depth are used to analyze the difference between the residual stress estimated by the function and the residual stress values measured by X-ray diffraction at each depth.

III. EXPERIMENTAL METHOD

A. Material and processes

Four cylindrical samples of the same low carbon steel were heat treated and machined in different ways. The composition, heat treatments, and machining processes cannot be detailed due to confidentiality reasons. These treatments and machining processes were applied in order to induce different residual stress-depth profiles on the samples while preserving the same ferrite-pearlite structure and hardness for all samples and depths.

B. Destructive measurements

The residual stress depth-profiles were measured by means of X-ray diffraction (XRD) using the $\sin^2\psi$ method. A Bruker D8 Advance diffractometer with a parallel beam polycap, PSD detector and Cr radiation (wavelength $\lambda = 2.291$ Å) was employed for these measurements. In order to measure the depth profile, it is necessary to successively remove layers of the material without further changing the residual stress state of the material. The best way to do this is by electrolytic polishing.[28] This method introduces the smallest modification in the stress state, although obviously it produces a slight stress relaxation. To take this relaxation into account, the layer removal correction proposed by Moore and Evans[29] can be applied. Nevertheless, in the present study, this correction is practically zero, because it is necessary to eliminate layers that are millimeters thick to obtain a noticeable correction, and in this work, the maximum depth reached after the removal of several layers is below 300 μm.

Qualitative characterization of the microstructures was carried out using optical (LEICA CTR 6000) and SEM

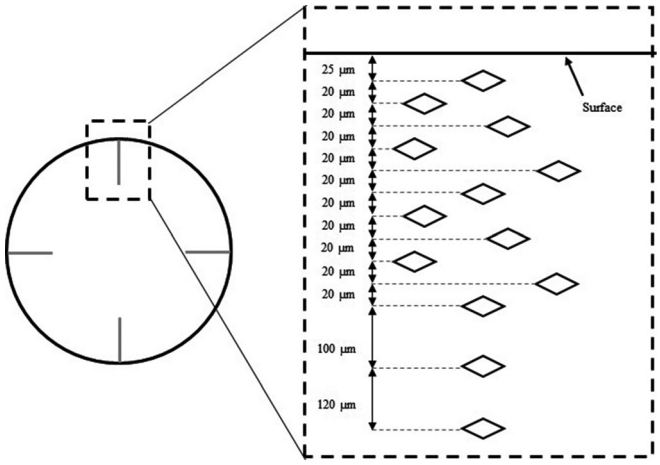

FIG. 1. Scheme of the cross section area of the cylinders with the microhardness depth-profiles performed every 90° and in the detail the Knoop microhardness pattern used to measure the microhardness at the surface of the four samples.

(FEG-SEM JOEL JSM-7000F) microscopic images. For this purpose, cross sections of the cylindrical samples were cut, polished, and etched in Nital 2% during 10 s for observation by optical and SEM microscopy.

Moreover, microhardness of the surface and core of the samples was measured using the Knoop method with a load of 0.1 kg during 5 s before etching the samples with a microhardness testing machine (Qness A30+). The microhardness measurements at the surface were performed in the cross section of the cylinders every 20 μm starting at a depth of 25 μm with the pattern shown in Fig. 1, to leave enough distance between indentations. This microhardness depth-profile pattern was repeated every 90° of the cross section in each sample.

C. MBN measurements

The MBN measurements were performed with a MBN measurement system developed at the Ceit-IK4 Technology Center. The details of the measurement system are found in Ref. 9. The cylindrical samples with different residual stress depth-profiles were excited under a varying magnetic field of 2 Hz created by a sinusoidal waveform current of amplitude ±0.6 A, passing through a coil wired to a ferromagnetic yoke, which produced a maximum applied magnetic field measured at the surface of the sample of around 10 000 A/m. The MBN signals were acquired by a surface induction sensor with a ferrite core and located at the surface of the sample. The acquired MBN was amplified by 60 dBs and high–pass filtered at 8 kHz. The MBN was acquired using a NI DAQ card with a 1 MHz sampling frequency. Each measurement consisted of 10 magnetizing cycles (5 s). The acquired signal was post-processed with a Matlab script. This script removed the first cycle because it was not stationary, then, it calculated the MBN magnitude spectrum [see Fig. 2(a), the continuous lines] by a fast Fourier transform for each cycle in the region where the MBN peak was present [the region between the vertical discontinuous lines shown in Fig. 2(b)], smoothed each spectrum by a moving average filter to calculate the envelope of the MBN magnitude spectrum, and finally the smoothed magnitude spectrum of each cycle was averaged [see the example in Fig. 2(a), the discontinuous line].

IV. DESTRUCTIVE CHARACTERIZATION

A. Residual stress depth profiles

The residual stress depth-profiles obtained by a combination of XRD measurements and electrolytic polishing in the longitudinal direction of the cylindrical samples (along the direction of the length of the cylinder) are shown in Fig. 3. All the samples present compressive stresses on the surface in the range between −250 MPa and −400 MPa. In the layer between 10 μm and 100 μm, the stress level of sample S1 increases from highly compressive stress (−270 MPa) up to slightly compressive stress (−50 MPa) and then it remains constant. Sample S2 increases its stress level from −300 MPa at the surface to –90 MPa at 20 μm, then the next measurement

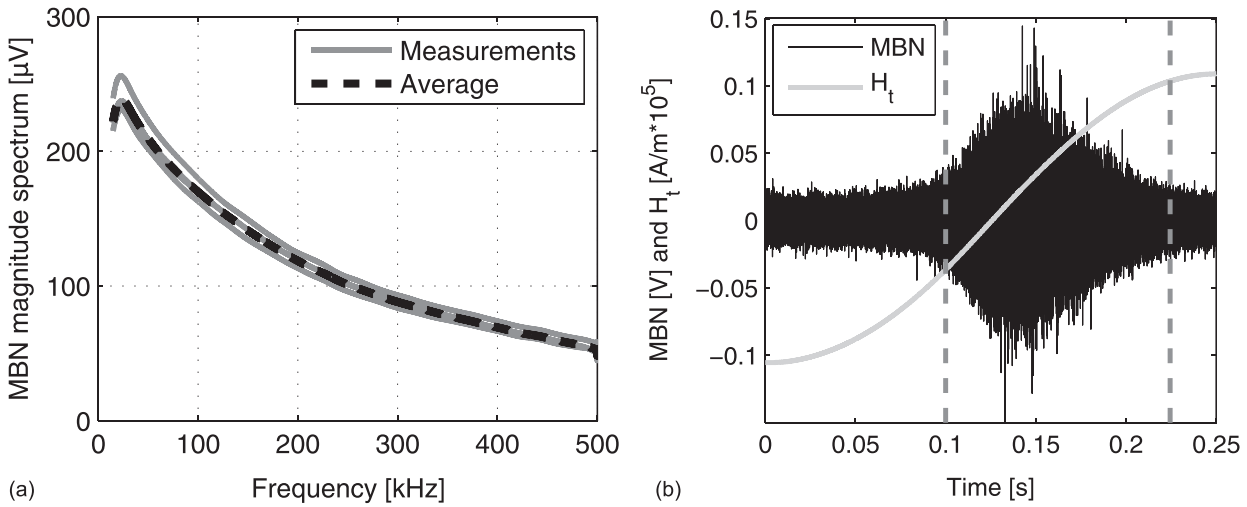

FIG. 2. (a) MBN magnitude spectrum of the peak area of each MBN cycle (continuous lines) and the average value of these MBN magnitude spectrum measurements (discontinuous line). (b) MBN and tangential magnetic field (H_t) signals and the peak region (between discontinuous vertical lines) which is used in the FFT to calculate the MBN magnitude spectrum.

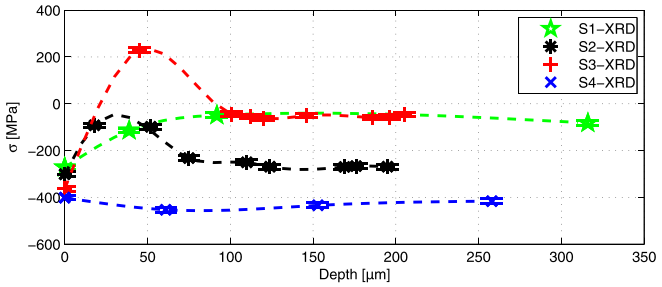

FIG. 3. Residual stress depth-profiles of the samples obtained by a combination of XRD and electrolytic polishing. The markers correspond to the actual measurements and the discontinuous lines are the splines calculated from these points. Error bars for each point represent the standard deviation of each measurement.

point at 50 μm presents a similar compressive stress level and starts decreasing slightly until −230 MPa at 70 μm and then it remains constant at greater depths. Sample S3 undergoes a large increase from an initial residual stress value of −400 MPa towards a tensile stress of 230 MPa at 50 μm, and then from 50 μm to 100 μm, the stress drops to slightly compressive stress values of around −50 MPa. Sample S4 keeps a high compressive stress value (larger than −400 MPa) for all the depths, with a small peak of a slightly larger compressive stress at 60 μm.

B. Microstructural evaluation

The microstructure observed by the optical microscope within the first 225 μm below the surface presents a ferrite perlite microstructure in all the samples, with a negligible change on the grain size, and phase percentage between the samples [see Figs. 4(a)–4(d)]. Furthermore, the microstructure for different depths within each sample presents little or no change with the exception of samples S3 and S4, which present some directionality in the first 1–2 μm. In Figs. 5(a) and 5(b), more detailed SEM micrographs for samples S1 and S3 of the first 65 μm below the surface are presented. It can be seen that the change in the microstructure along the depth is also negligible, apart from the directionality present in the first 1–2 μm.

C. Microhardness measurements

Figures 6(a)–6(d) show the microhardness measurements for the four samples at the first 400 μm from the surface. It can be seen that there is no significant variation in the hardness both along the depth and between the different samples. These microhardness values are equivalent to approximate hardness Rockwell C values between 23 and 25 HRC both at the surface, subsurface, and at the core of the four samples.

V. APPLICATION OF THE APPROACH FOR ESTIMATING RESIDUAL STRESS DEPTH-PROFILES

In this section, the approach proposed in Sec. II B is applied using both the extended and the bare Kypris-Jiles models. The application of the approach for the extended model is presented in detail and then, the residual stress depth-profile estimations obtained with the extended model are compared with the estimations obtained from the bare model.

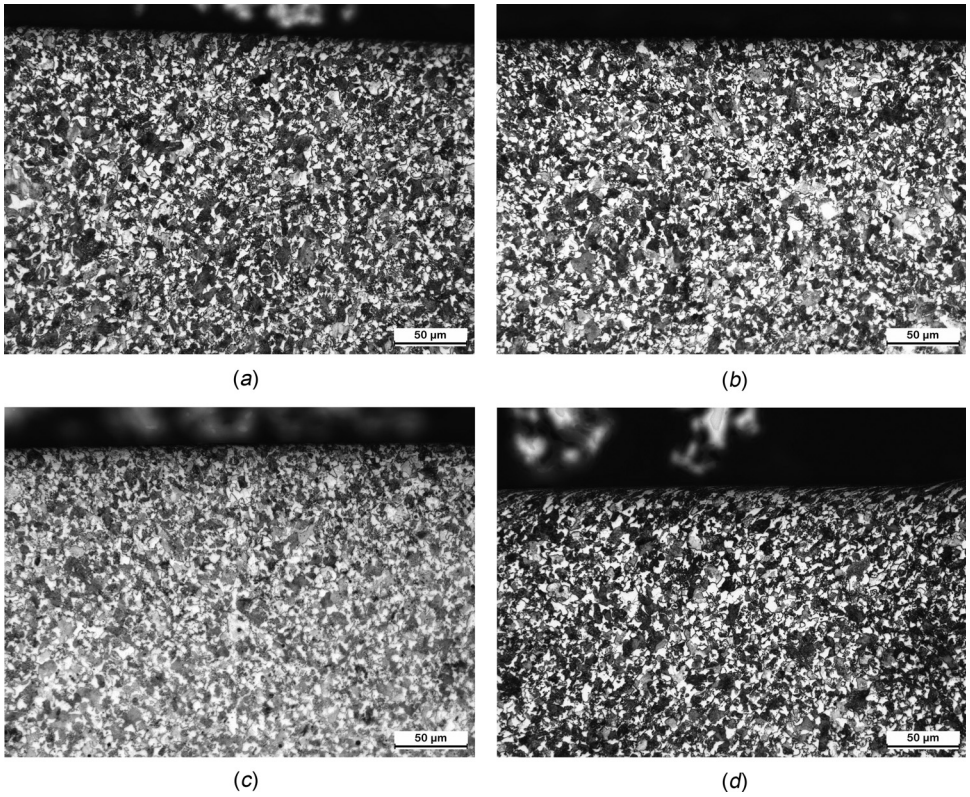

FIG. 4. Optical micrograph from the surface to a depth of 225 μm of samples (a) S1, (b) S2 (c) S3 and (d) S4 (etched with nital 2%).

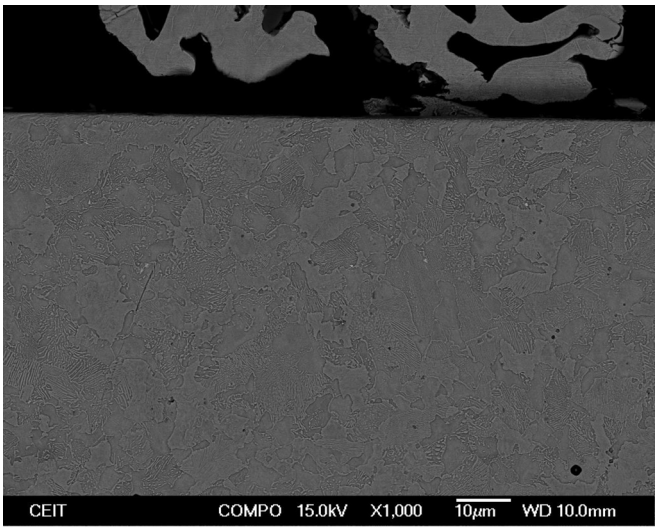

(a)

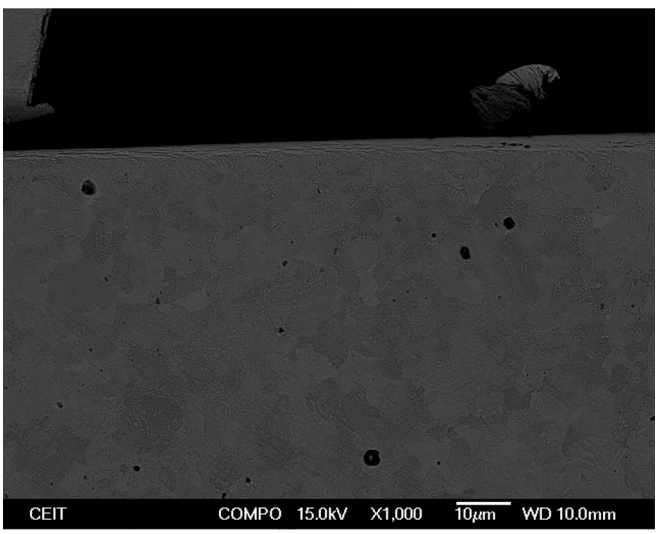

(b)

FIG. 5. SEM micrograph from the surface to a depth of 65 μm of samples (a) S1 and (b) S3 (etched with nital 2%).

A. Application of the approach with the extended Kypris-Jiles model

1. Fitting the extended Kypris-Jiles model to the measured MBN magnitude spectrum

In Fig. 7(a), the MBN magnitude spectra of the samples are shown. It can be seen that the spectra present a peak at low frequencies. This behavior is normal in the MBN magnitude spectrum,[30,31] but Eqs. (5) and (8) cannot model the region of the spectrum with a peak, only the region where the spectrum continuously decreases. Therefore, in the present study, the magnitude spectrum in the region between 25 kHz [marked with the vertical black line in Fig. 7(a)] and 500 kHz is used for the fitting. As the minimum frequency used is 25 kHz, by considering ρ and μ to be similar to the iron ones (0.3175 $\mu\Omega$ m and 500*μ_0, respectively[22,23]), the skin depth, δ, is around 80 μm; this means that the x_{n-1} value for the present approach is 140 μm, whose depth is 1.8 times greater than the value of the skin depth, δ.

In the present study, the MBN magnitude spectrum measured is described by 475 frequency points. Thus, there are 475 equations to solve by the nonlinear least squares fitting in Eq. (8). Considering the width of the layers, Δx, 10 μm, and given the minimum depth, x_0, is 0 μm and the maximum depth, x_{n-1}, is 140 μm, the unknown parameters are 15 V_{orig} values, 14 ζ values and the value of parameter k.

Figure 7(a) illustrates the average MBN magnitude spectra measured at the surface of the samples, shown as continuous lines, and the fitting curves obtained after adjusting the parameters of the model [Eq. (8)] by a nonlinear least squares fit, shown as discontinuous lines. Distinct values of residual stress depth-profiles in the samples lead to different spectrum shapes with varying peak amplitudes for the MBN measured at the surface, as predicted by simulations of the Barkhausen spectrum emanating from diverse stress-depth profiles.[11] The relative errors between the measured and the fitted average MBN magnitude spectra are represented in Fig. 7(b). It can be seen that there are deviations with respect to the real spectrum, especially in the 25–60 kHz and 400–500 kHz frequency bands.

The V_{orig} values from 10 μm to x_{n-1} (140 μm) at different layers (V_{orig} depth-profile) of each of the samples obtained from the fitted model are shown in Fig. 8. The V_{orig} value of depth x = 0 is not taken into account since this parameter also takes within it the random Gaussian noise introduced by the measurement.[10] It can be seen that the V_{orig} depth-profiles of samples S1, S2, and S3 present a peak in the region of around 30 μm–50 μm depth, and then the V_{orig} values decrease steadily. On the contrary, the V_{orig} values for sample S4 decrease slightly and continuously from the surface to 140 μm deep.

2. Comparison of V_{orig} parameters and residual stress depth-profile

In order to get a good relation between residual stresses and V_{orig} values at each depth, it is necessary that the hypothesis taken to derive Eq. (8), i.e., that the microstructure presents a negligible effect on the V_{orig} should be true. In the present study, it has been seen that the phase (ferrite and perlite) percentage, grain size, directionality, and microhardness for the four samples in the analyzed depth (between 10 μm and 140 μm) does not change significantly. In the literature, it has been seen that the influence of the dislocation density could be negligible comparing to the change of the residual stresses in some materials.[7,16] Therefore, for the present comparison, the hypothesis taken in Ref. 10, that the V_{orig} is only influenced by residual stresses at each depth, is still assumed.

Hence, if the V_{orig} depth-profile results are compared with the residual stress depth-profiles presented in Fig. 3 and taking into account that tensile residual stresses increase the MBN signal amplitude and that compressive stresses decreases the MBN signal amplitude,[3–10,13,15] it can be seen that the shape of the V_{orig} values as a function of the depth and the shape of the residual stress depth-profiles show great resemblance. In the region from 10 μm to 50 μm (1st region, marked by a green border in Fig. 8), the shapes of the V_{orig}

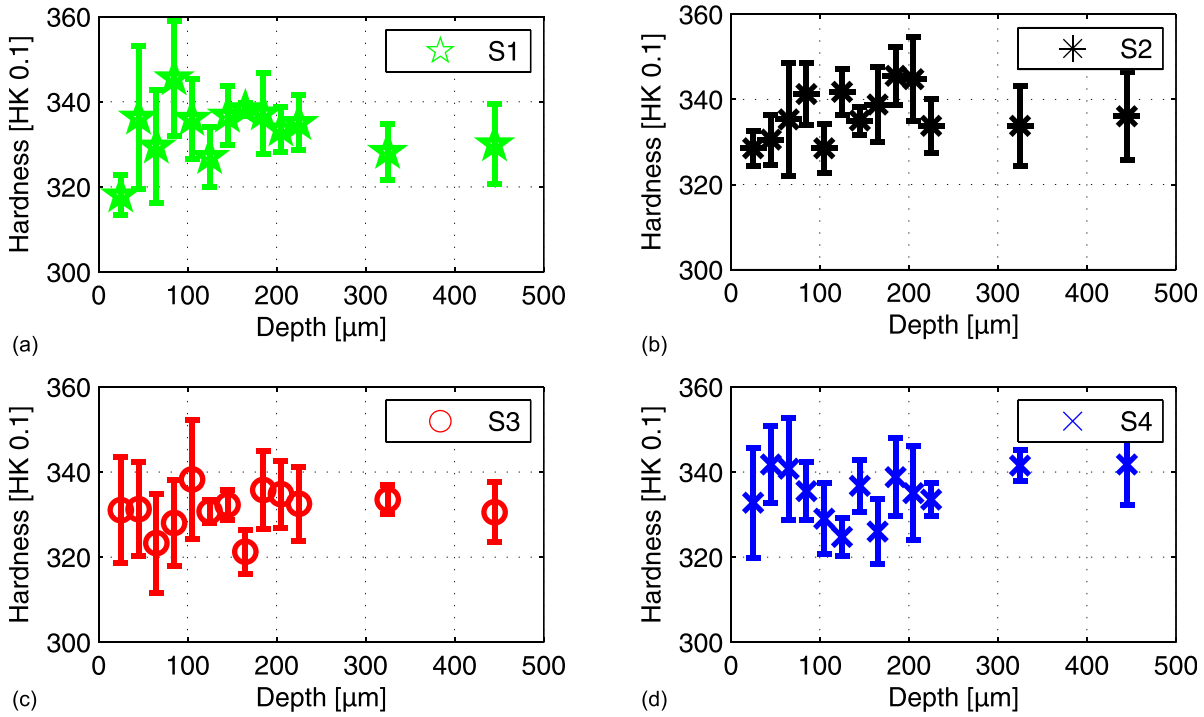

FIG. 6. Knoop microhardness measurements in the cross section along the depth in samples (a) S1, (b) S2, (c) S3 and (d) S4. The average value and standard deviation calculated from the four microhardness depth-profile patterns performed every 90° for each depth are shown.

values of all samples accurately match the residual stress depth-profile, the V_{orig} values increasing when the stress increases toward more tensile (S1 and S3 in 50 μm depth and S2 in 30 μm depth) and the V_{orig} values decreasing when the stress decreases to more compressive (S2 from 30 μm to 50 μm and S4 in this 50 μm depth). From a depth of 50 μm to 140 μm (2nd region, marked by a red border in Fig. 8), the V_{orig} values decrease when residual stresses do not decrease or decrease faster than residual stresses do, and the resemblance to the residual stress is worse. However, in this region, the relation between the V_{orig} values of the different samples match the relation between the residual stress values of the samples at these depths: the stress values and the V_{orig} values of samples S1 and S3 became similar after 100 μm, while the difference between samples S2 and S4 decreases and samples S1 and S3 present higher V_{orig} values and more tensile values than samples S2 and S4. Thus, it looks as though all samples were multiplied by the same function that depends on the depth and that the effect of the function has a greater impact on the V_{orig} values located at deeper depths. The loss of resemblance between the V_{orig} and the residual stress depth-profiles for greater depths makes sense with the error observed between the fitted and the measured MBN magnitude spectrum [see Fig. 7(b)], which shows great

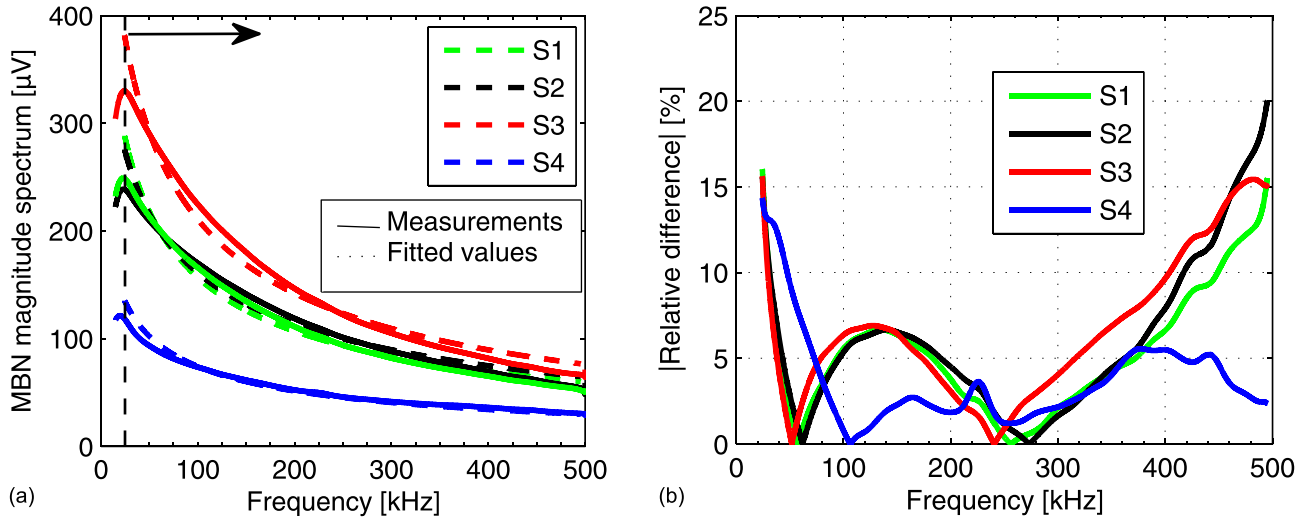

FIG. 7. (a) MBN magnitude spectrum obtained by real measurement (continuous) and by the extended model of the MBN magnitude spectrum (discontinuous line) for all samples. The discontinuous vertical line indicates the minimum frequency used in the fitting. (b) Relative difference for each frequency of the MBN magnitude spectrum between the measured data and the data estimated by the extended model.

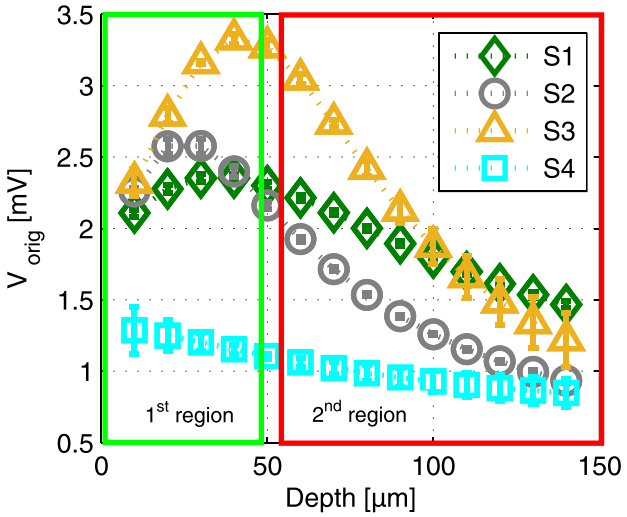

FIG. 8. MBN amplitudes emitted at the origin of different depths (V_{orig} depth-profile) for the studied samples obtained from the fitting of the extended model. The green border indicates a region that goes from the surface to a depth of 50 μm and the red border indicates a region going from 50 μm deep up to 140 μm deep. Error bars for each point represent the standard deviation of each measurement.

difference in the lower frequencies, where the MBN emitted at greater layers has a higher impact on the total value. The deviation of the V_{orig} depth profile from the residual stress depth-profile could be due to the fact that some effects have been oversimplified to obtain Eq. (8) such as considering the emission of the MBN as a white noise (it is possible that it would present a spectrum between the white noise and the Brownian noise spectra due to a magnetization rate lower than predicted by parameter c) or taking the effect of the MBN due to the exponential attenuation of the applied magnetic field dependent on the eddy current attenuation, to be linear.

Therefore, it can be seen that the V_{orig} values obtained with this approach have good qualitative resemblance with the residual stress depth-profiles, especially in the first 50 μm, and the relation between the V_{orig} values and the residual stress values is good at all the depths. Therefore, an idea of the differences in the residual stress depth-profiles between samples can be gained by only measuring the MBN magnitude spectrum on the surface and applying the fitting of the model proposed here.

3. Calibration and validation

In the present study, samples S1, S3, and S4 were used to obtain the calibration functions and sample S2 was employed for the validation of these functions. However, it has to be emphasized that in the present case, choosing other samples for calibration and validation does not change the estimated residual stress depth-profile significantly. Figures 9(a), 9(b), and 9(c) show examples of calibration functions for 20 μm, 90 μm, and 130 μm. The equations of these functions [shown inside boxes in Figs. 9(a), 9(b), and 9(c)] are obtained by matching the V_{orig} values calculated from the extended model at each x_n depth (Fig. 8) to the residual stress values at the same x_n depth (Fig. 3), obtained from the splines from the residual stress values measured by the

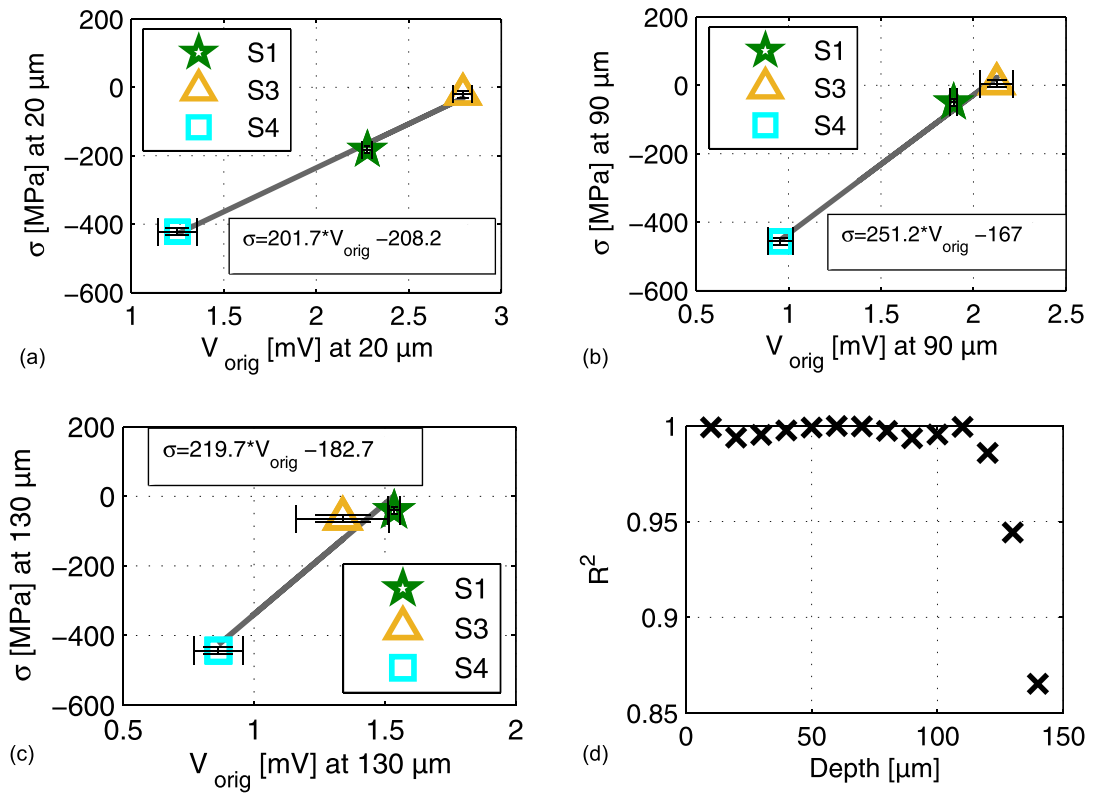

FIG. 9. Residual stress versus the V_{orig} of samples S1, S3 and S4 (markers), calibration function (continuous grey line) and the equation of the calibration functions (equation inside a box) on the depths of (a) 20 μm (b) 90 μm and (c) 130 μm. (d) Coefficients of determination, R^2, for the calibration functions obtained at each depth. Error bars for each point represent the standard deviation of each measurement.

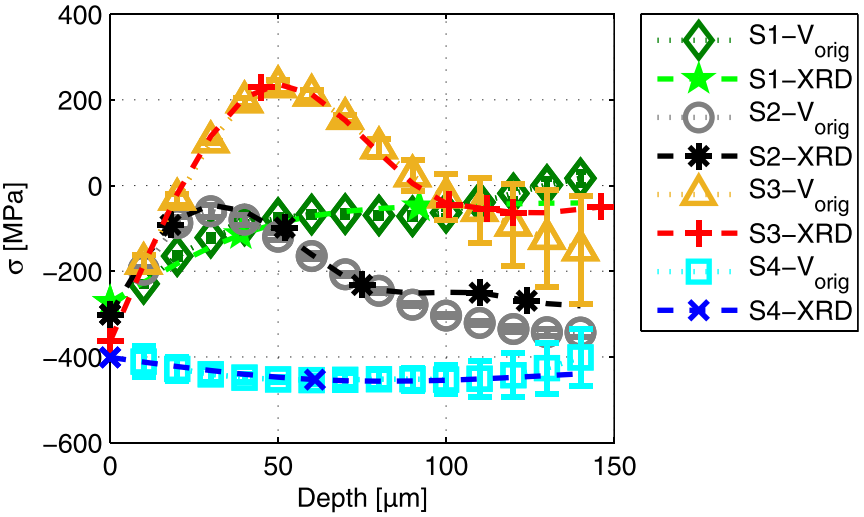

FIG. 10. Residual stress-depth profiles of the samples obtained by XRD and electrolytic polishing (XRD in legend) and residual stress-depth profiles of the samples obtained using the extended approach proposed here (V_{orig} in the legend). The markers and the discontinuous lines of the XRD correspond to the XRD and electrolytic polishing measurement and the splines, respectively, and the markers and dotted lines of the MBN correspond to the calculated values and the interpolations between these points, respectively. Error bars for each point represent the standard deviation of each measurement.

combination of XRD measurement and electrolytic polishing. All these functions have positive slopes; that is, an increase in the stress causes an increase in the V_{orig} values. This is expected due to the relation between the MBN amplitude and the stress, which produces higher MBN amplitudes when the stress is more tensile.[3–10,13,15] The coefficients of determination, R^2, of all the calibration functions obtained in all the depths are represented in Fig. 9(d). It can be seen that the coefficients of determination are above 0.98 for all the depths up to 120 μm, when it decreases to values around 0.85.

In order to validate if these functions obtained for each depth, relating the expected residual stress with the V_{orig} value at each depth, are capable of estimating the profiles of other samples and therefore to validate the proposed model and approach, the V_{orig} values of sample S2 (validation sample) are introduced in the equations representing the functions of each depth to estimate the residual stress depth-profile and then to compare this estimated depth-profile with the residual stress depth-profile measured by a combination of XRD and electrolytic polishing (see Fig. 10). It can be seen that the estimated residual stress depth-profile obtained from the surface MBN measurements is very similar to the measured residual stress depth-profile for all the depths, with an error of estimation smaller than 30 MPa from the surface up to a depth of 90 μm below the surface and at deeper depths, up to 140 μm, the deviations from the measured residual stress values are smaller than 70 MPa.

In addition, in Fig. 10, the residual stress depth-profiles measured by a combination of XRD and electrolytic polishing and the residual stress depth-profiles estimated by the calibration functions [the ones presented in equation form in Figs. 9(a), 9(b), and 9(c)] with the values of the V_{orig} for the samples S1, S3, and S4 (used to obtain calibration functions) are also shown.

These residual stress depth-profile estimations show that the extended approach proposed in the present paper is valid to estimate nonmonotonic residual stress depth profiles with an error smaller than 30 MPa, up to a depth of 90 μm, and smaller than 70 MPa, up to a depth of 130 μm below the surface. The extended approach considers the hypotheses made in the bare Kypris-Jiles model and the new ones: adding the effect on the MBN due to magnetic field attenuation; defining the maximum depth analyzed (x_{n-1}) as 1.8*δ; selecting V_{orig} as the parameter representing punctual changes in material properties; and doing a linear calibration stage to relate the V_{orig} with the residuals stresses at each depth.

B. Comparison of estimated residual stress depth-profiles with the bare and extended Kypris-Jiles model

When the same procedure was carried out but using the bare Kypris-Jiles model [with $x_{n-1} = \delta$ as proposed in Ref. 10, 80 μm in this material], worse results were obtained in both qualitative and quantitative estimation of residual stress depth-profiles. In Fig. 11, it can be seen that the V_{orig} depth-profiles present a similar shape between each other, but do not present any resemblance with the shape of the residual stress depth-profiles measured by a combination of XRD and electrolytic polishing (Fig. 2). Therefore, only from the V_{orig} depth-profiles obtained with the extended model (Fig. 8), it

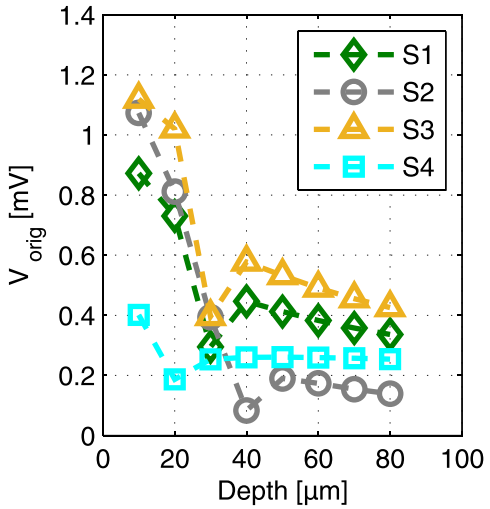

FIG. 11. MBN amplitudes emitted at the origin of different depths (V_{orig} depth-profile) for the studied samples obtained from the fitting of the bare Kypris-Jiles model.

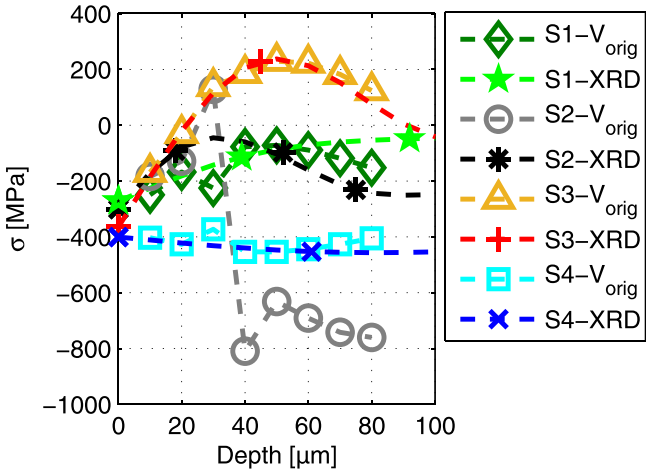

FIG. 12. Residual stress-depth profiles of the samples obtained by XRD and electrolytic polishing (XRD in legend) and residual stress-depth profiles of the samples obtained using the bare Kypris-Jiles approach (V_{orig} in the legend). The markers and the discontinuous lines of the XRD correspond to the XRD and electrolytic polishing measurement and the splines, respectively, and the markers and dotted lines of the MBN correspond to the calculated values and the interpolations between these points, respectively.

is possible to obtain qualitative information of the residual stress depth-profile.

Furthermore, the estimated residual stress depth-profile obtained after the calibration process on the validation sample (S2) obtained with the bare Kypris-Jiles model is very different from the residual stress depth-profile measured by XRD for all the depths, with an estimation error greater than 500 MPa, as can be seen in Fig. 12. This error is much larger than the error of 70 MPa obtained with the extended model up to 130 μm (Fig. 10). Hence, it can be concluded that the improvements introduced in the extended model are necessary to estimate nonmonotonic residual stress depth-profiles.

VI. CONCLUSION

An extended approach based on the Kypris-Jiles model of the Barkhausen magnitude spectrum is proposed to estimate nonmonotonous residual stress depth-profiles. The main change of the extended model is the addition to the Kypris-Jiles model the effect of the attenuation of the magnetic field on the MBN. The V_{orig} depth-profiles (MBN amplitude at different depths) obtained from fitting the extended model of the Barkhausen magnitude spectrum to the measured spectra, give qualitative information about the residual stress depth-profiles independent of the shape of the residual stress depth-profile, improving the results obtained with the bare Kypris-Jiles model. Calibrating and validating the V_{orig} depth-profiles obtained with the extended Kypris-Jiles model with the residual stress depth-profiles at each depth, results in a good quantitative estimation of the residual stress depth-profiles up to 130 μm, with an error smaller than 70 MPa.

Therefore, the extended approach proposed in the present study enables a nondestructive estimation of the nonmonotonous residual stress depth-profiles that could be applied in-situ or in production lines. Moreover, this approach could be valid for estimating other properties of the material along the depth that influence the MBN amplitude. The application of this approach in a wide range of applications where the estimation of residual stresses via a nondestructive testing technique is required is promising. It is also a starting point for other applications, where not only residual stress depth-profiles but also microstructure or hardness depth-profiles need to be estimated, such as case hardening characterization or microstructure gradients in laminated steel.

ACKNOWLEDGMENTS

We would like to express our thanks to Virginia García Navas, formerly at the IK4-TEKNIKER Technology Center, for her help with the sample preparation and for performing the XRD measurements and to Nerea Burgos from the Ceit-IK4 Technology Center for her help with the sample preparation and for performing optical and SEM micrographs.

[1]W. Z. Zhuang and G. R. Halford, "Investigation of residual stress relaxation under cyclic load," Int. J. Fatigue **23**, 31–37 (2001).
[2]C. You, M. Achintha, K. A. Soady, N. Smyth, M. E. Fitzpatrick, and P. A. S. Reed, "Low cycle fatigue life prediction in shot-peened components of different geometries—Part I: Residual stress relaxation," Fatigue Fract. Eng. Mater. Struct. **40**, 761–775 (2017).
[3]P. Jacob, S. Marrone, L. Suominen, and V. Honkamaki, "Non-destructive evaluation of residual stress depth-profiles by Barkhausen noise analysis and their validation by XRD method combined with electrochemical (destructive) surface removal," in *4th International Conference on Barkhausen Noise and Micromagnetic Testing, Brescia (Italy)* (2003), p. 361.
[4]V. Moorthy, B. A. Shaw, and S. Day, "Evaluation of applied and residual stresses in case-carburised En36 steel subjected to bending using the magnetic Barkhausen emission technique," Acta Mater. **52**, 1927–1936 (2004).
[5]S. Desvaux, M. Duquennoy, J. Gualandri, and M. Ourak, "The evaluation of surface residual stress in aeronautic bearings using the Barkhausen noise effect," NDT&E Int. **37**, 9–17 (2004).
[6]S. Desvaux, M. Duquennoy, J. Gualandri, M. Ouaftouh, and M. Ourak, "Evaluation of residual stress profiles using the Barkhausen noise effect to verify high performance aerospace bearings," Nondestr. Test. Eval. **20**, 9–24 (2005).
[7]X. Kleber and A. Vincent, "On the role of residual internal stresses and dislocations on Barkhausen noise in plastically deformed steel," NDT&E Int. **37**, 439–445 (2004).
[8]X. Kleber and S. P. Barroso, "Investigation of shot-peened austenitic stainless steel 304L by means of magnetic Barkhausen noise," Mater. Sci. Eng., A **527**, 6046–6052 (2010).
[9]A. Lasaosa, K. Gurruchaga, V. García Navas, and A. Martínez-de-Guereñu, "Characterisation of in-depth stress state by magnetic Barkhausen noise on machined steel acquiring different frequency bands," Adv. Mater. Res. **996**, 373 (2014).
[10]O. Kypris, I. C. Nlebedim, and D. C. Jiles, "A model for the Barkhausen frequency spectrum as a function of applied stress," J. Appl. Phys. **115**, 83906 (2014).
[11]O. Kypris, I. C. Nlebedim, and D. C. Jiles, "Barkhausen spectroscopy: Non-destructive characterization of magnetic materials as a function of depth," J. Appl. Phys. **115**, 17E305 (2014).
[12]L. P. Mierczak, Y. Melikhov, and D. C. Jiles, "Determining residual stress depth profiles using the magnetic barkhausen effect," IEEE Trans. Magn. **50**, 1–5 (2014).
[13]P. Vourna, A. Ktena, P. E. Tsakiridis, and E. Hristoforou, "A novel approach of accurately evaluating residual stress and microstructure of welded electrical steels," NDT&E Int. **71**, 33–42 (2015).
[14]O. Kypris, I. C. Nlebedim, and D. C. Jiles, "Measuring stress variation with depth using Barkhausen signals," J. Magn. Magn. Mater. **407**, 377–395 (2016).
[15]M. A. Campos, J. Mewis, and E. G. D. Conte, "In-situ magnetic inspection of the part fixture and the residual stress in micromilled hot-work tool steel," NDT&E Int. **90**, 33–38 (2017).

[16]L. Piotrowski, M. Chmielewski, and Z. L. Kowalewski, "The dominant influence of plastic deformation induced residual stress on the barkhausen effect signal in martensitic steels," J. Nondestr. Eval. **36**, 10 (2017).
[17]S. Santa-aho, M. Vippola, A. Sorsa, K. Leiviskä, M. Lindgren, and T. Lepistö, "Utilization of Barkhausen noise magnetizing sweeps for case-depth detection from hardened steel," NDT&E Int. **52**, 95–102 (2012).
[18]V. Moorthy, "Important factors influencing the magnetic Barkhausen noise profile," IEEE Trans. Magn. **52**, 1–13 (2016).
[19]D. C. Jiles, "Magnetization and magnetic moment," in *Introduction to Magnetism and Magnetic Materials*, edited by D. C. Jiles (Chapman & Hall, Boca Raton, 1998), Vol. 2, p. 119.
[20]M. Blaow, J. T. Evans, and B. A. Shaw, "Effect of hardness and composition gradients on Barkhausen emission in case hardened steel," J. Magn. Magn. Mater. **303**, 153–159 (2006).
[21]M. Vashista and V. Moorthy, "On the shape of the magnetic Barkhausen noise profile for better revelation of the effect of microstructures on the magnetisation process in ferritic steels," J. Magn. Magn. Mater. **393**, 584–592 (2015).
[22]S. Chikazumi, *Physics of Magnetism* (Wiley, New York, USA, 1964), Vol. 1.
[23]J. Woolman and R. A. Mottram, *The Mechanical and Physical Properties of the British Standard EN Steels* (Pergamon Press, 1966), Vol. 2, p. 390.
[24]O. Saquet, J. Chicois, and A. Vincent, "Barkhausen noise from plain carbon steels: Analysis of the influence of microstructure," Mater. Sci. Eng., A **269**, 73–82 (1999).
[25]A. Stupakov, M. Neslušan, and O. Perevertov, "Detection of a milling-induced surface damage by the magnetic Barkhausen noise," J. Magn. Magn. Mater. **410**, 198–209 (2016).
[26]V. Moorthy, B. A. Shaw, P. Mountford, and P. Hopkins, "Magnetic Barkhausen emission technique for evaluation of residual stress alteration by grinding in case-carburised En36 steel," Acta Mater. **53**, 4997–5006 (2005).
[27]L. Mierczak, D. C. Jiles, and G. Fantoni, "A new method for evaluation of mechanical stress using the reciprocal amplitude of magnetic Barkhausen noise," IEEE Trans. Magn. **47**, 459–465 (2011).
[28]ASM International, "Electrolitic Polishing," in *Metallography and Microstructures*, edited by K. Mills (ASM International, USA, 1992), pp. 48–56.
[29]M. G. Moore and W. P. Evans, "Mathematical correction for stress in removed layers in X-ray diffraction residual stress analysis," SAE Technical Paper 580035 (1958).
[30]G. Durin and G. Bertotti, "Barkhausen noise in FeCoB amorphous alloys," J. Appl. Phys. **79**, 5142 (1996).
[31]G. Durin and S. Zapperi, "On the power spectrum of magnetization noise," in *Proceedings of the Joint European Magnetic Symposia (JEMS'01)* (2002), Vol. 242–245, pp. 1085–1088.